JOURNAL OF MATERIALS SCIENCE **34** (1999) 5789–5802

The influence of metals and carbides during laser surface modification of low alloy steel

M. H. McCAY, N. B. DAHOTRE, J. A. HOPKINS, T. D. McCAY
University of Tennessee Space Institute, Tullahoma, Tn 37388, USA
E-mail: cthomas@utsi.edu

M. A. Riley
Surface Treatment Technology, Tullahoma, TN 37388, USA

The addition of both elements (Cr and Ni) and carbides (SiC and WC) during laser surface alloying under different processing speeds produced surfaces with both enhanced hardness wear resistance and corrosion properties compared to the base AISI 4340 steel material. These effects were due to the evolution of unique microstructures within the laser-processed region, which includes austenite, ferrite, martensite, Fe- and Si-based carbides and the retention of the original carbides (SiC and WC) in various combinations. The chromium and nickel stabilized the austenite and ferrite but reduced the formation of martensite that is useful to increase the hardness and prevent cracking. Also, the substantial dissociation of the original carbides (SIC and WC) into elemental silicon and tungsten supplemented the stabilization of ferrite and reduction in the hardness. The presence of the undissociated carbides and some martensite formation provided substantial increases in the microhardness. The improvement of both the mechanical properties and corrosion resistance might be self-exclusive due to the reduction of the carbides and the subsequent inability of the matrix to prevent cracking.

1. Introduction

The extensive variety of materials now available provide the engineer with the freedom to select those with adequate, if not superlative, properties. But just as the variety of materials has expanded, so has the multitude of applications, once again pushing the limits of the available materials and challenging the materials scientist. One complication, which is becoming more obvious as facilities and components age, is surface degradation by corrosion and wear. This is true in particular for many metallic alloys, and when such materials are placed in a hostile environment, extensive degradation can result with its associated problems. For large-scale structures, this means a very difficult decision and trade-off between base mechanical properties and surface properties.

Among the many solutions proposed for surface protection is laser surface alloying [1–4], a technique whereby the high energy of a laser is used to introduce additional elements to a thin surface layer, producing a new alloy. In order to cover large surfaces, the laser beam is displaced by a distance (the index) to create a series of overlapping melt pools or tracks. This is shown schematically in Fig. 1, which also shows the precursor containing the alloying elements on the surface of the substrate and a cross-section of the tracks. During the laser surfacing process, the laser melts the substrate and alloys the precursor elements into the melt pool forming the surface alloy. This new surface then protects the base material, which maintains its desirable mechanical properties. The promise of such a combination of properties has made the idea of laser surface alloying very interesting and generated significant research in the previous decade. Unfortunately, while the concept of laser surface alloying is straightforward, the practice is fraught with complications due largely to the myriad responses of the base material to both the alloying elements and the energy input. Both equilibrium and non-equilibrium phases can occur [5, 6], depending on a variety of processing parameters among which are percentage of alloying element addition, energy input and melt layer depth. As a result, the success of the technology is strongly dependent upon the understanding and control of these parameters.

The addition of chromium and nickel to iron base alloys is generally known to improve corrosion resistance and so has been utilized in laser surface alloying as a means of producing a corrosion-resistant surface on a less resistant substrate alloy. During the laesr surface alloying process, the intense energy(10^6 W/cm^2) of the laser melts a thin (10–1000 μm) surface region of the substrate, enabling the addition of elements such as chromium and nickel through means of powder injection or a slurry mix. Once resolidified, the result is a base material with its original properties but protected by a surface that is corrosion resistant. Alloying additions and original alloy constituents dictate the final composition while laser processing parameters such as input power and dwell time dictate the equilibrium and non-equilibrium phase formation.

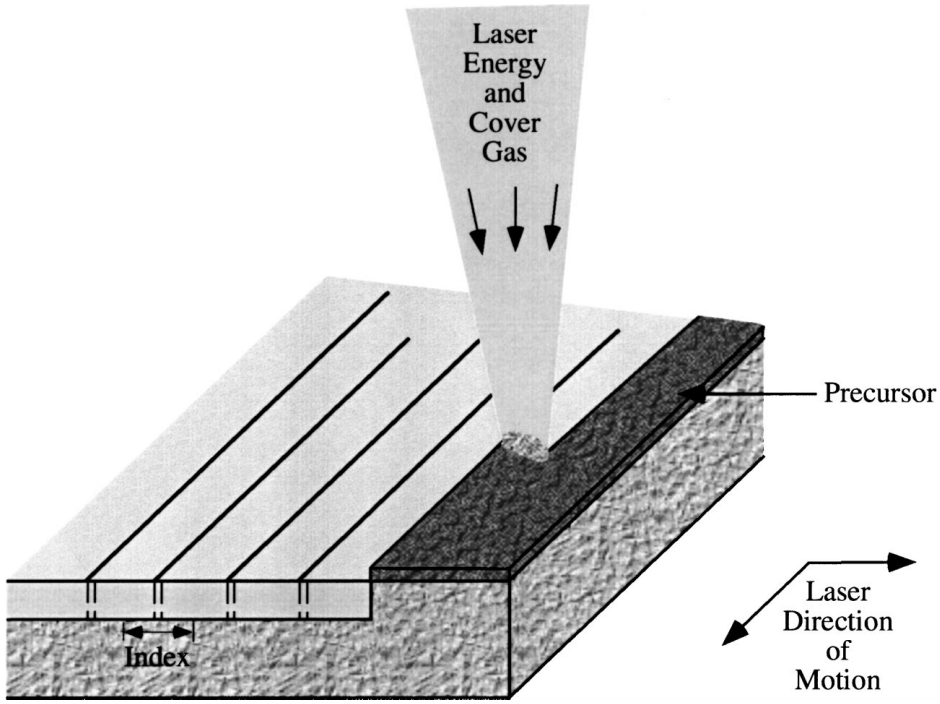

Figure 1 A schematic of the laser surfacing process.

Numerous examples exist of surface alloying to obtain corrosion resistance, one such [7] involved feeding chromium and nickel powder into the melted region of 1016 steel to obtain surface compositions ranging from 22.1 wt % Cr/17.2 wt % Ni to 37.6 wt % Cr/21.8 wt % Ni. There were no cracks on the processed surface, and corrosion tests results implied that the samples were mechanically and metallurgically sound. After spontaneously passivating in 3.5 NaCl solution, the laser alloyed surfaces had a current density about the same or less than that of 304 stainless steel. In this example, as well as others [5], there was evidence of chromium rich precipitates as well as chromium carbides.

Another study [8] in which chromium and nickel were placed on the surface in a slurry and alloyed into 1010 and A36 steel showed that corrosion protection could be obtained while producing a variety of steel phases by varying the composition with the processing parameters. The phases present were predicted from the Schaeffler diagram [9] using compositional analysis of the layers and the overall hardness was then predictable using weighted hardness values for the individual phases. Wear results were explained based on the phase percentages.

Further examples exist in which carbides of tungsten and silicon have been laser surface infiltrated with steels to produce greater hardness and wear resistance. When tungsten carbide was incorporated by powder injection with a low (0.14–0.19 wt %) carbon steel [10], dissolution and reprecipitation of the particles occurred at high intensities (greater than 2×10^4 W/cm^2) accompanied by significant cracking and porosity. When the powder injection and associated carbide content was kept very low, then the cracking and porosity were reduced, and the hardening occurred through martensitic transformation enhanced by carbon enrichment from the carbide. At very high powder injection rates, the cracking and porosity were again reduced, but since the WC had not dissolved, it contributed to both the hardness and wear resistance. When SiC was added to Incoloy 800H [11], the hardness of the surface modified layer also showed an increase after treatment. In this case the carbide was found to have dissociated during melting with the resultant precipitation of M_7C_6 carbides.

The primary objective of this study was to examine the combined effects of the addition of chromium, nickel and carbides on the properties of a laser processed surface. As discussed above, the addition of the elements chromium and nickel enhance corrosion resistance, particularly when the chromium exceeds 12 wt %, making them desirable additions to the surface of a steel material. They also dictate predictable phase changes, with chromium being a ferrite former and nickel an austenite former, therefore, reducing the hardening due to martensitic transformation. These phase alterations can produce a significant secondary effect in the surface alloy by reversing the residual stresses from the compressive stresses expected in a martensitic surface to the tensile stresses in an austenite surface [12, 13]. The carbides, on the other hand, increase the hardness and wear resistance, but their chemistry must be considered during processing since their decomposition can alter the steel phases by supplying either carbon, which is an austenite former, the individual elements of tungsten and silicon, which are ferrite formers, or new carbides. The dissociation of the carbide additives is a strong possibility during laser processing with its intense energy density. For example, although WC is chemically rather stable, it decomposes into its components above 2600 °C [14], a temperature well within the regime of laser surface processing. This potential dissociation generates the secondary objective of this study which is to determine if the surface alloy properties can be predicted using the Shaeffler diagram and hardness values for the phases and carbides.

TABLE I Composition (wt %) of Alloy 4340

Alloy	C	Mn	Si	Ni	Cr	Mo
4340	0.38–0.43	0.6–0.8	0.2–0.35	1.65–2	0.7–0.9	0.2–0.3

2. Experimental procedure

Steel coupons of 4340 steel (6 by 76 by 154 mm) were used as substrates for these experiments. The composition is given in Table I. The 4340 steel was selected for this study because it is generally the standard to which other ultrahigh strength steels are compared and combines hardenability with ductility, toughness and strength. In addition, it has good strength at elevated temperatures and is readily heat-treatable.

The large surfaces of the substrates were sandblasted and then coated with a slurry comprised of chromium (44 wt %), nickel (22 wt %), silicon carbide (3 wt %) and tungsten carbide (8 wt %) powder, varnish and mineral spirits. Once the slurry had dried at room temperature, processing was accomplished in air with a CW 3 kW Hobart Nd : YAG laser at an overlap index of 2.5 mm at 2000 W and 1000, 1500, 2250 and 3000 mm/min. This varied the interaction time for each set. For baseline purposes, an uncoated sample of 4340 was processed using 2000 W and 1500 mm/min.

3. Specimen preparation and material characterization

Subsequent to processing, the sample surfaces were examined optically for signs of cracking. Each was then cut into pieces for more extensive analysis. One sample each was selected for polishing and metallurgical analysis. This consisted of mounting and then polishing on emery papers up to 600 grit and then with 2–4 μm diamond paste. They were etched with Nital to distinguish the melt interface for depth measurements and with a mixture of methanol and aqua regia to view the microstructure within the layer. Knoops microhardness measurements (500 gms @ 15 s) were taken within the layer, the heat affected zone and the base material in 20 μm increments using an automated microhardness tester. The presence of cracking within the surface layer was noted. Energy dispersive spectroscopy (EDS) (standardless, background removed) analysis was used for determination of the chromium, nickel, silicon and tungsten content. Using a second set of samples, further analysis was conducted with X-ray diffraction (CuK_α, 1.54 Å wavelength radiation), first on the as-processed surface, then on the same with 100 μm of the surface removed.

Other properties of interest were ascertained by corrosion testing in a Q-Fog chamber (ph 6.5–7.2, 5 wt % NaCl, 35 °C, 100% relative humidity) for 24 h and two sets of wear testing (block-on-disc apparatus at 1000 rpm (280 m/min) and 4 lbs. normal weight) to determine weight loss/minute and friction coefficient after 2, 10 and 20 min.

4. Results and discussion

A compilation of the characterization results is given in Tables II and III (average values). The samples (A, B, C, and D) are presented in order of increased processing speed. Comparison data for 4340 processed (E) and as-received (F) is also given.

4.1. Surface and cross-section analysis

All of the sample surfaces had some evidence of surface micro-cracking (see Fig. 2) indicative of residual stresses.

From the average compositional analysis of the cross-sections (Table II), it can be seen that the chromium and carbide contents vary inversely to the depth of the layers. The nickel content, however, remains at 2%, which is around the limit of accuracy of the analysis technique. The cracking increased in severity from Set A to D (Table III), with D containing the highest amount of inclusion induced fracture sites. Set A had relatively little cracking which occurred primarily at the midpoint of the beam track. Sets C and D had extensive cracking exhibiting extremely brittle failure and penetrating the depth of the processed region. There was some porosity in the samples generally associated with agglomerates of the carbides and indicating incomplete precursor mixing.

4.2. Microstructural analysis

In order to examine the relative roles of phases and carbides in contributing to the mechanical properties, the chromium and nickel equivalents were determined using the averaged wieght percents of chromium and nickel in the processed region, along with a calculated value of the amount of carbon present (assuming dilution from alloying). Following that, the percentage of the martensite, austenite and ferrite phases in each sample were estimated from the Schaeffler diagram [9] and are given in Table III.

TABLE II

Set	Speed (mm/min)	Layer depth (μm)	Average hardness (Knoops)	Average composition (rem Fe) Cr wt %	Ni wt %	Si(C) wt %	W(C) wt %	Total carbides (wt %)	Carbide/iron/silicon phase (1 → 4)
A	1000	462	576 ± 64	10.2	2	7.5	4.2	11.7	(Least) 1
B	1500	315	634 ± 59	12.4	2	8.7	5.2	13.9	2
C	2250	231	644 ± 97	13.3	2	9.1	6.3	15.4	3
D	3000	246	741 ± 161	17.9	2	12.2	8.4	20.6	(Most) 4
E(4340P)	1500		590	0.8	1.8	0	0	0	
F(4340)			270						

TABLE III

Set	Cracking severity (1→4)	Crack location	Predicted Schaeffler phases			Observed phases
			Martensite vol %	Ferrite vol %	Austenite vol %	
A	Least (1)	Overlap	91	0	9	Austenite/ferrite
B	2	Mid track	68	0	32	Austenite/ferrite
C	3	Both	60	0	40	Austenite/ferrite
D	Most (4)	Both/chunks	10	4	86	Austenite/ferrite
E			100	0	0	Martensite/ferrite

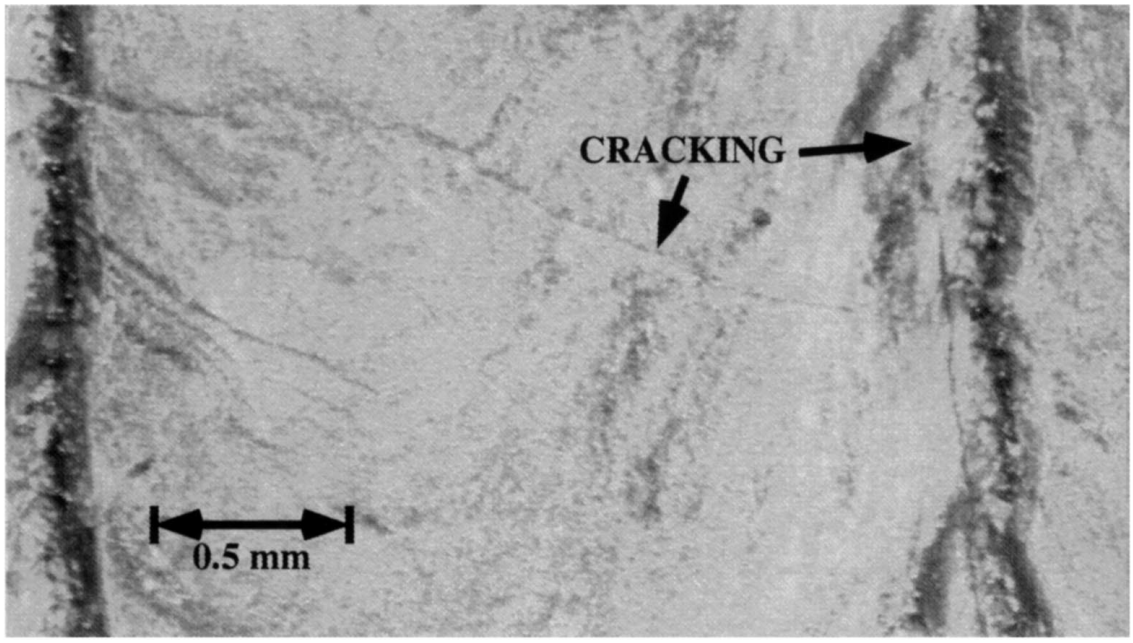

(a)

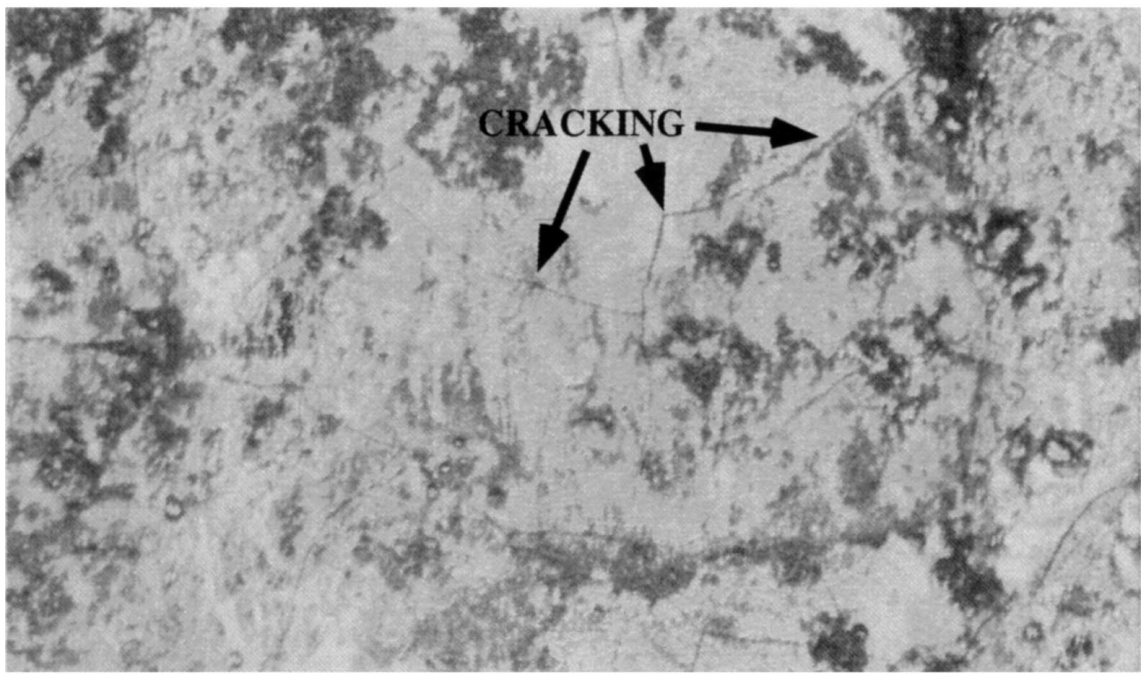

(b)

Figure 2 Surface cracking after processing at 2000 W and (a) 1000 mm/min, sample A and (b) 2250 mm/min, sample C.

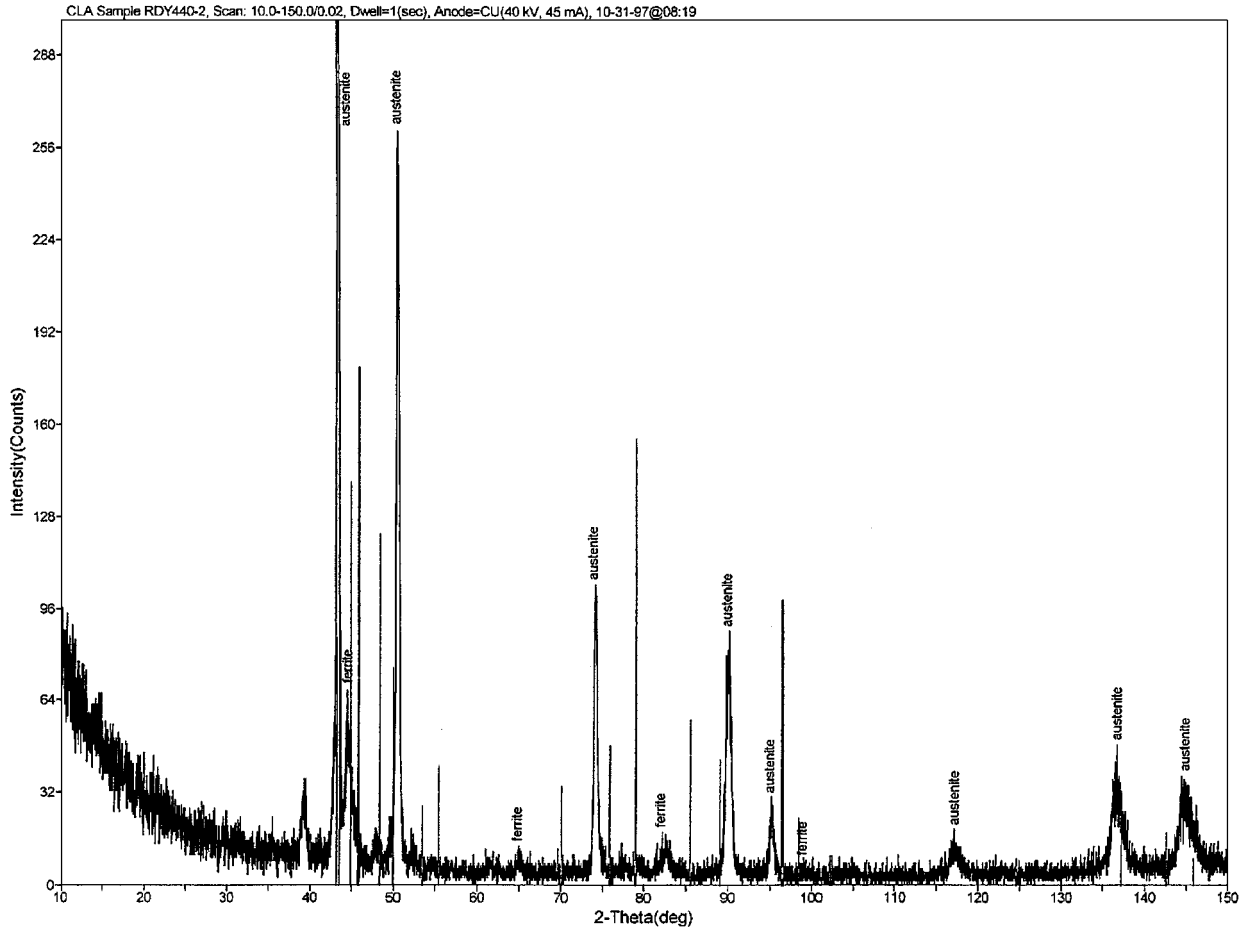

Figure 3 X-ray diffraction scan of surface of sample A.

Observations using standard microscopy and three different etchants (Nital, Kallings I and Kallings II) showed that contrary to what was expected from the Schaeffler predictions, sample A contained significant austenite indicating a shift toward higher carbon, while the remaining samples had noticeable ferrite content, indicating the predictions using the Schaeffler diagram should be shifted toward higher chromium equivalents and therefore more ferrite. While the Schaeffler diagram takes into account the contribution of the chromium additive to the ferrite formation and nickel to the austenite formation, it was unable to include the individual silicon, tungsten and dissociated carbon contributions, since the extent of their presence due to dissociation of the carbides was unknown. It is helpful as an indicator however by showing that the individual elements will drive the phases towards a combination of austenite and ferrite.

The application of X-ray diffraction for quantitative phase determination was hampered, since diffracted intensities from all four sets were low as a result of surface roughness and curvature. A scan for Set A is given in Fig. 3 and demonstrates the significant austenite present. X-ray scans of the remaining samples also showed both austenite and ferrite phases. The relative strength and the leftward shift of the austenite peaks suggest that these have high chromium content. Indications of any remaining un-dissociated SiC and WC were very weak but sample D evidenced a large amount of SiC-5H. In addition, when the surfaces of the samples were removed, the remaining layers all strongly indicated the presence of a carbon-iron-silicon (12, 79, 9 at %) phase suggesting a dissociation of the incorporated silicon carbide and a non-stoichiometric composition of Si-C compound. The degree of occurrence of this newly formed carbide is given in Table II and indicates the possibility that some elemental silicon, which is a ferrite former, was present in the alloyed layer. Since both silicon and tungsten are soluble in iron up to around five and six weight percent, it wasn't possible to distinguish their presence in dissociated form other than by their influence on the phase formation.

4.3. Mechanical property analysis

As seen in Table II, the average microhardness varies inversely with the layer depth. The standard deviation is also given, so an appreciation can be gained for the extent of inhomogeneity within the sets, which is also reflected in the microhardness maps shown in Fig. 4. (Note that light regions indicate high hardness.) Fig. 5 shows sample C before and after microhardness testing and the significant cracking which occurred as a result of the testing process. This effect did not occur in samples A and B but pre-dominated in sample D to the extent that a surface map was not possible. An estimate of cracking severity and location is also given in Table III and substantiates the microhardness data, in that severity increases from sample A to D. The regions of lower hardness (dark) are primarily in the midtrack

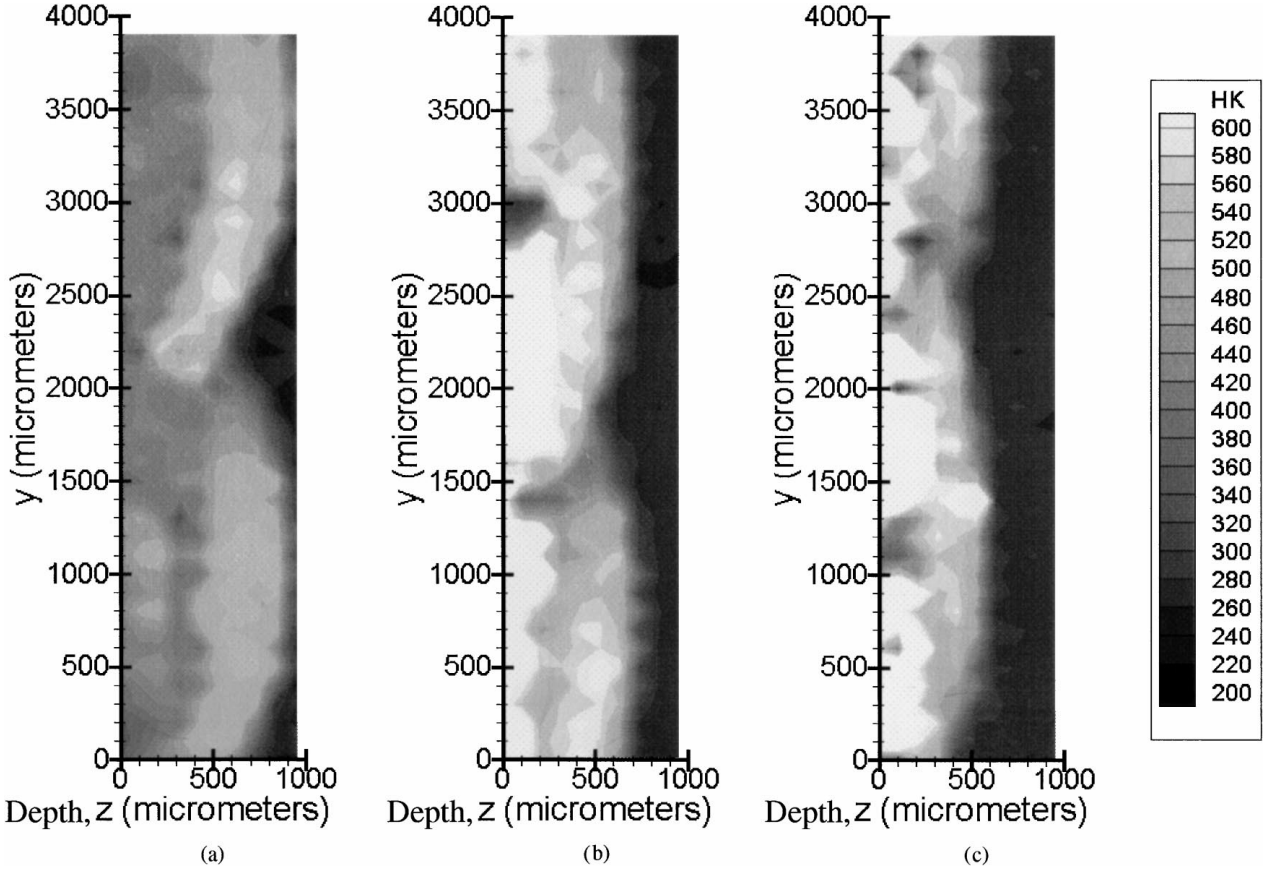

Figure 4 Microhardness maps of samples (a) A, (b) B, and (c) C, showing the cross-section depth perpendicular to the surface, ($z = \phi$ is the surface).

or overlap areas which also are the locations where cracking occurs.

A plot of average microhardness vs. the total silicon plus tungsten percent (Fig. 6) reveals a linear relationship which when curve-fit yields the following:

$$\text{Microhardness} = 373 + 17.9\,(\text{wt\% carbides})$$

Using this relationship between hardness and weight percent silicon plus tungsten, the hardness of the silicon plus tungsten additives can be calculated to be 2100 Knoops, an acceptable value for carbides based on the literature [15]. The matrix material (zero w + si), however, has a Knoops hardness of significantly lower than the hardness of sample E, the processed matrix material with no alloying addition. Sample E's value of 590 Knoops is in keeping with predictions for transformed 4340 with approximately 100% martensite. All of this suggests that the microhardness is essentially independent of the matrix phase percentages and is dominated by the carbide additions whether they remain the original carbides or not. This is not to say that the phases are insignificant with regard to other properties. For example, the severity of cracking is greatest when there is the least predicted martensite.

Wear test results are given in Fig. 7, which gives the grams lost per minute over a ten minute period for the base 4340(F), as well as the processed 4340(E) and the sample surfaces. In two of the samples (A and D), the addition of chromium, nickel and the carbides increased the wear over the processed and unprocessed base material. In samples B and C the wear was slightly less than the base. The friction coefficients as a function of time are given in Fig. 8, and the relationship between friction coefficient (at 20 min) and the carbide content of the samples is given in Fig. 9.

The worn surfaces were further subjected to topographic observations using SEM (Figs 10–13) and X-ray diffraction analysis (Figs 14–17). The X-ray diffraction analysis was conducted to identify the evolution of new phases during the wear process. Such new phases, along with the prior-to-wear matrix phases in the laser-alloyed region, are expected to influence wear behavior.

Sample A has a large amount of martensite (91 vol %) in addition to austenite (9 vol %) as matrix. The martensite is a very hard and brittle phase which provides high hardness ($\sim R_c$ 50–55) to the alloyed region. Furthermore, the sample also contains a dispersion of a large amount of carbides (SiC + WC) (11.7 wt %). The hard carbides($> R_c$ 60) and the hard phase martensite together tend to sustain very high wear loads/forces. As both the hard phase (martensite) and hard carbide (SiC + WC) particles are surrounded by the relatively softer/ductile austenite phase, excessive wear loads/forces (>yield of the carbides and martensite) are dissipated and/or accommodated by plastic deformation of the austenite matrix. Such deformation of the material is a mixed mode of the types, mostly attrition and a little plowing, thereby providing maximum material losses during the wear (Fig. 7). Fig. 10 for sample A is indicative of such attrition dominated mixed mode wear mechanism. The debris due to fracture of brittle phase is sometimes buried within cohesive film formed by the plastically deformed soft phase matrix.

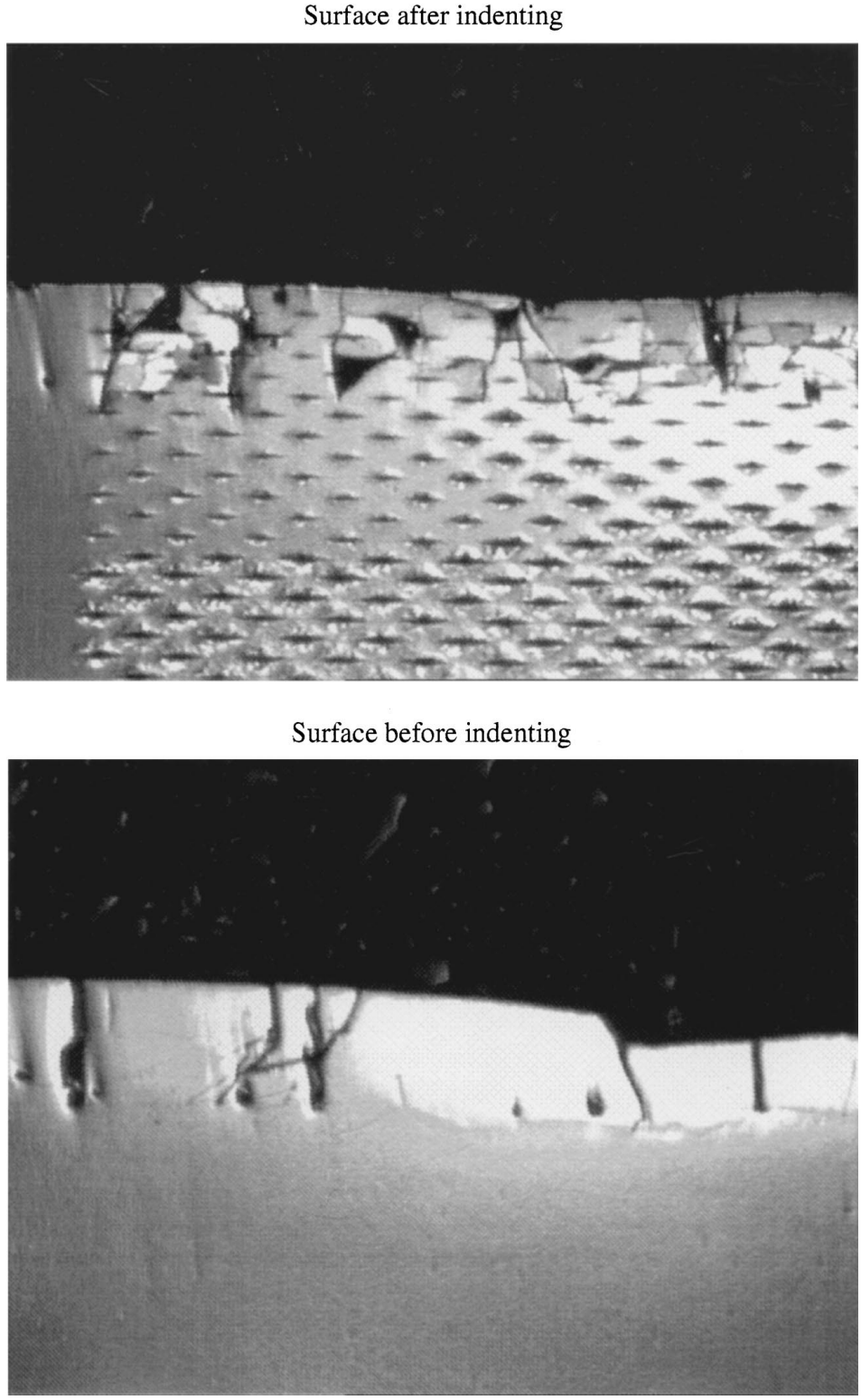

Figure 5 Cross-section views of sample C showing the extent of cracking which occurred during microhardness testing.

The matrix of samples B and C consists of a mixture of moderate amount of martensite (68 vol % and 60 vol %, respectively) and austenite phase (32 vol % and 40 vol %, respectively) that is infiltrated with the moderate amount (13.9 wt % and 15.4 wt %, respectively) of the mixture of carbides (SiC + WC). Such a combination provides a large enough volume of hard material (hard phase and/or carbide particles) to sustain equal wear forces, along with the soft matrix such as austenite ($\sim R_c$ 25–30) that tends to easily accommodate wear forces by undergoing extensive plastic deformation. This evenly mixed type (attrition + plowing) wear mechanism provides the optimum conditions under which the least loss of material occurs (Fig. 7). Figs 11 and 12 for samples B and C, respectively, illustrate surfaces produced during such a mixed type wear.

Sample D has an austenite (86 vol %) matrix which is infiltrated with the largest content (20.6 wt %) of the mixture of carbide particles (SiC + WC). Such a combination tends to provide on average high hardness

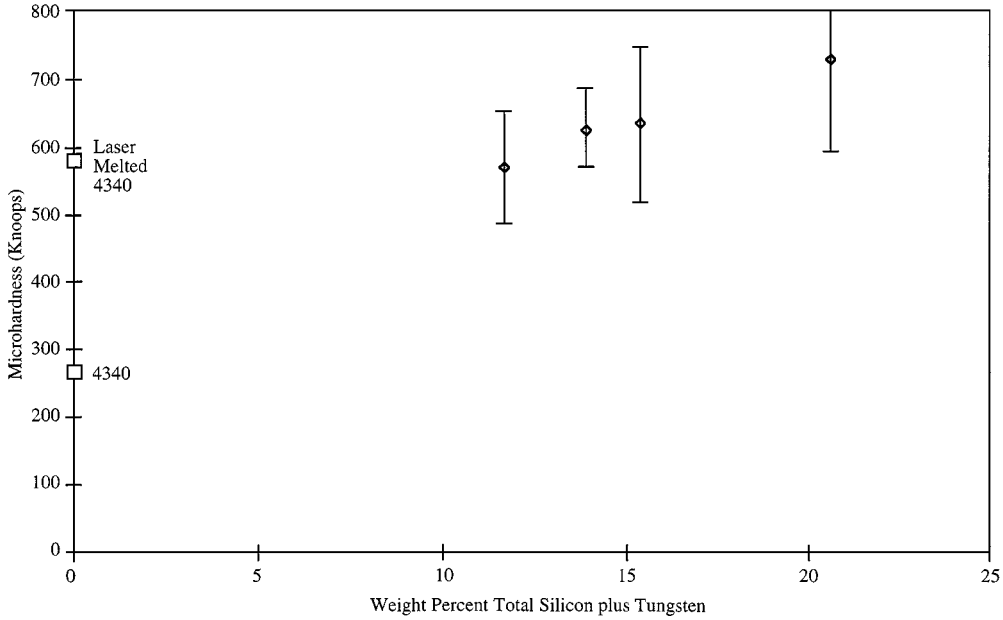

Figure 6 Plot of average Knoops microhardness vs. silicon plus tungsten weight percent.

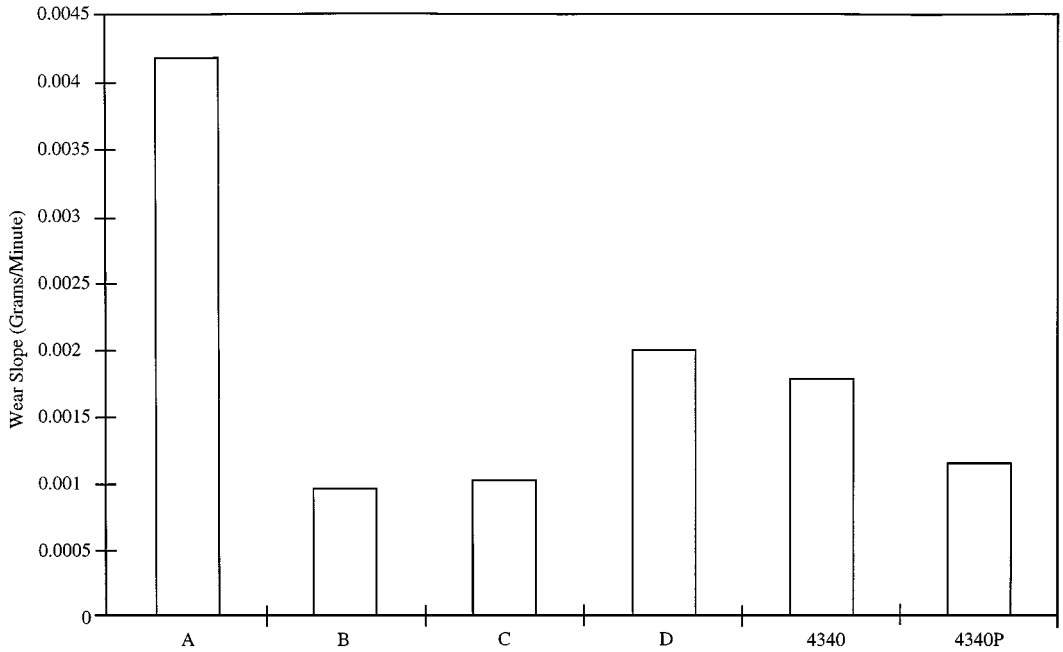

Figure 7 Wear slopes of processed and unprocessed 4340 samples (block-on-disc apparatus at 280 m/min and 4 lbs normal weight).

(741 Knoops) to the laser treated region. In general, a hard surface such as this is expected to withstand very high wear forces. However, the regions (pockets) containing a high concentration of carbides fracture due to wear forces. The fractured carbides in a ductile matrix of austenite come loose further to involve them in attrition wear. Due to such selective attritive wear, the average wear losses are moderate (Fig. 7). Fig. 13a illustrates two locations of brittle fracture due to attrition wear in sample D. Figs 13b and 13c are high magnification views of those two fractured locations from Fig. 13a showing intragranular cracks and faceted fractured surfaces.

As the coefficient of friction is a direct function of the work done to deform (elastically and/or plastically) the surface material, it is not necessarily a direct indication of material loss or separation as loose debris from the surface during wear. In view of this, Fig. 8 illustrates the behavior of the coefficient of friction over a period of 20 min of dry sliding wear testing. The break-in period during which asperities deform to provide large contact surface area for elastic/plastic deformation under equilibrium thermomechanical conditions is in the range of 120–400 s. The constant values of coefficient of friction for sample B ($\mu \cong 7.4$) and sample C ($\mu \cong 8.2$) lie between those for sample D ($\mu \cong 8.5$) and sample A ($\mu \cong 6.8$). Since sample A microstructure probably contains martensite, along with carbides (11.7 wt %), and since both phases are hard and brittle, sample A's surface does not undergo large elastic/plastic deformation. Instead, it experiences material loss by catastrophic failure; therefore, the work

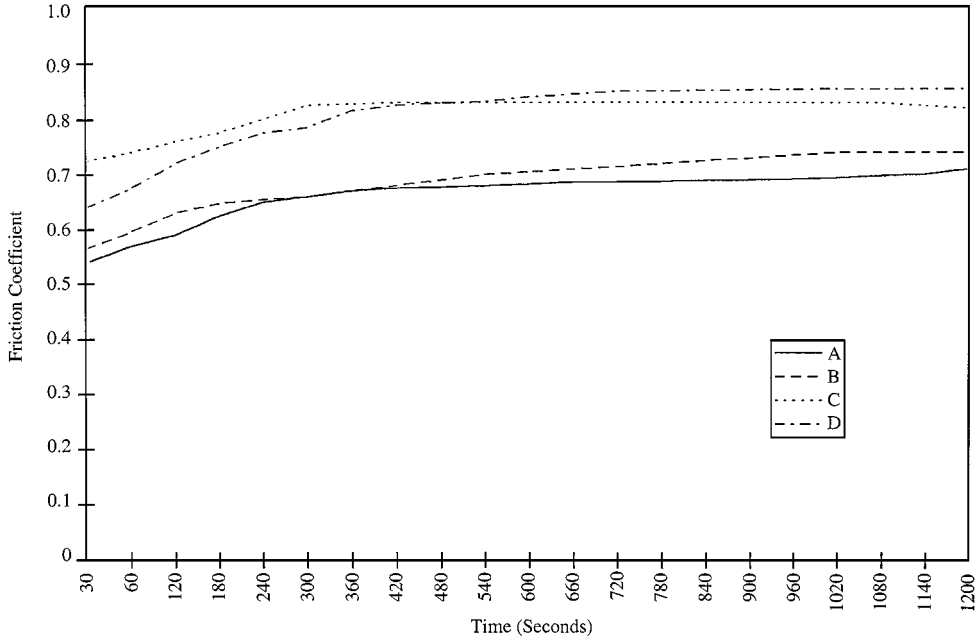

Figure 8 The coefficient of friction as a function of time.

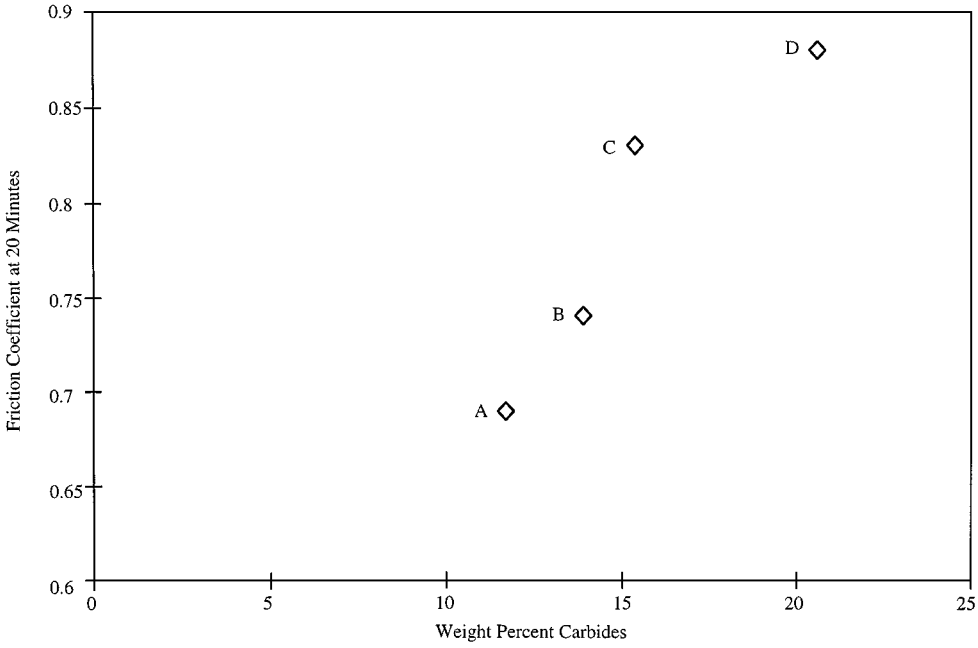

Figure 9 The coefficient of friction at twenty minutes shown as a function of the total carbide content.

expended during the wear and the constant coefficient of friction remain lowest compared to other samples (Fig. 13). On the contrary, sample D, even though it contains the largest amount of carbides, also contains the largest amount of austenite phase (86 vol %). Austenite is a very ductile phase which undergoes large deformation prior to its failure at (separation from) the surface which involves a large amount of work to be expended, thereby giving the highest value of the coefficient of friction (Fig. 13). Samples B and C, due to the presence of a combination of intermediate amounts of phases, possess intermediate values of coefficient of friction (Fig. 8).

Attempts were made using X-ray diffractometry to find out if any by-product is produced during the wear of these surfaces, since by-products tend to participate in the wear of the surfaces either in an adverse or beneficial manner. All spectra contained only the peaks corresponding to the original components (phases and particles) of the samples. It appeared that no new species were formed during wear.

4.4. Additional tests

None of the processed samples exhibited corrosion as a result of the fog chamber environment. This was expected for samples, B, C and D, since in all cases they contained more than 12 wt % chromium, although sample A had marginal chromium for protection. Based on X-ray diffraction results, it is possible that either magnetite or chromite appeared, but not rust.

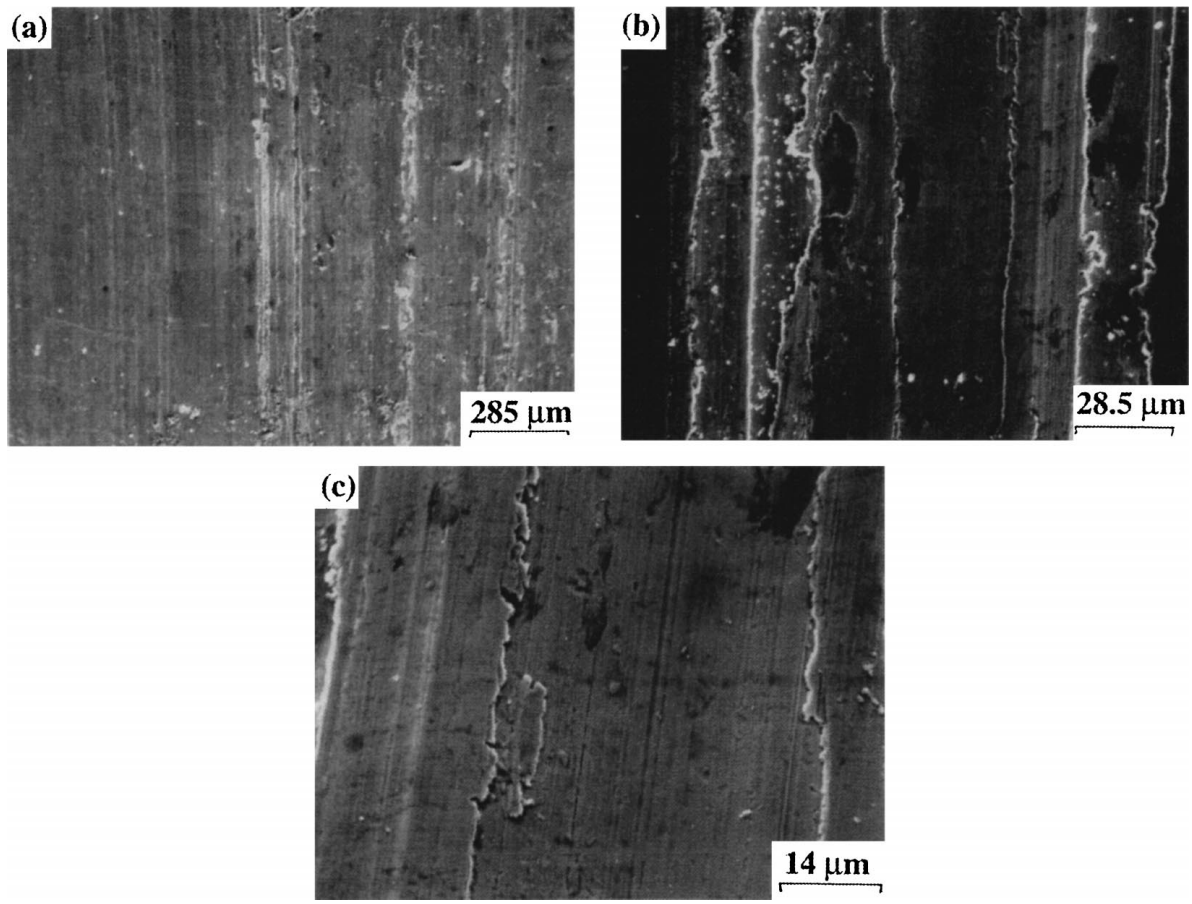

Figure 10 SEM micrographs of the sample A after it was subjected to dry sliding wear. Figures (b) and (c) are medium and high magnification views of the region in Figure (a).

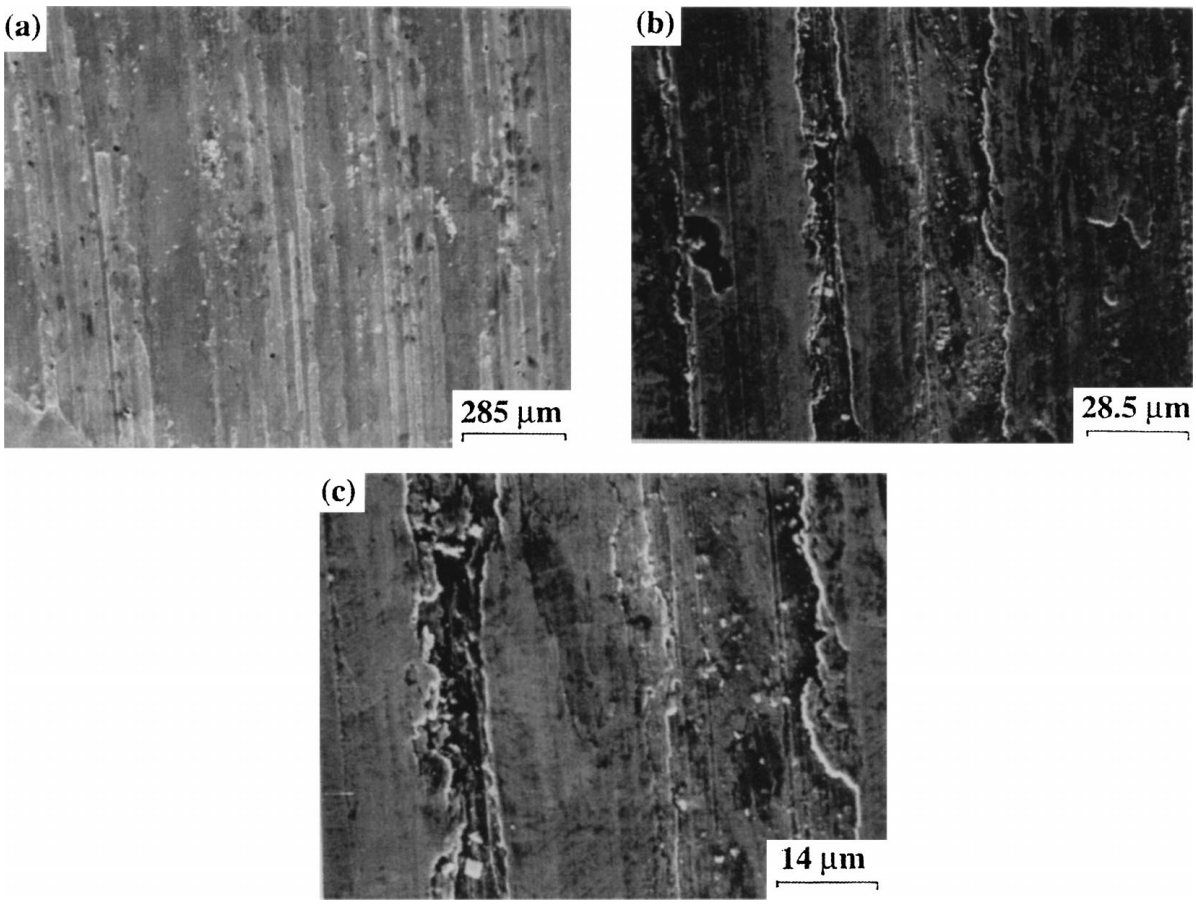

Figure 11 SEM micrographs of the sample B after it was subjected to dry sliding wear. Figures (b) and (c) are medium and high magnification views of the region in Figure (a).

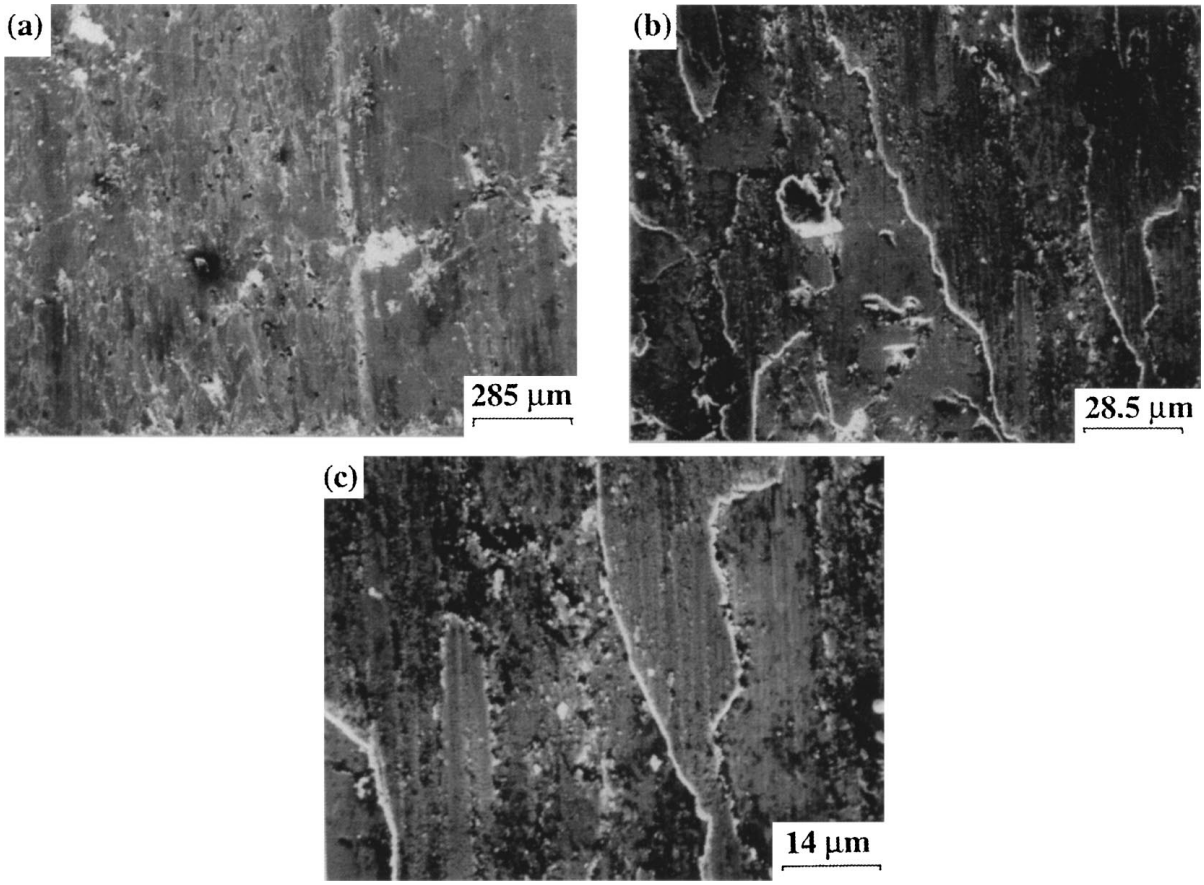

Figure 12 SEM micrographs of the sample C after it was subjected to dry sliding wear. Figures (b) and (c) are medium and high magnification views of the region in Figure (a).

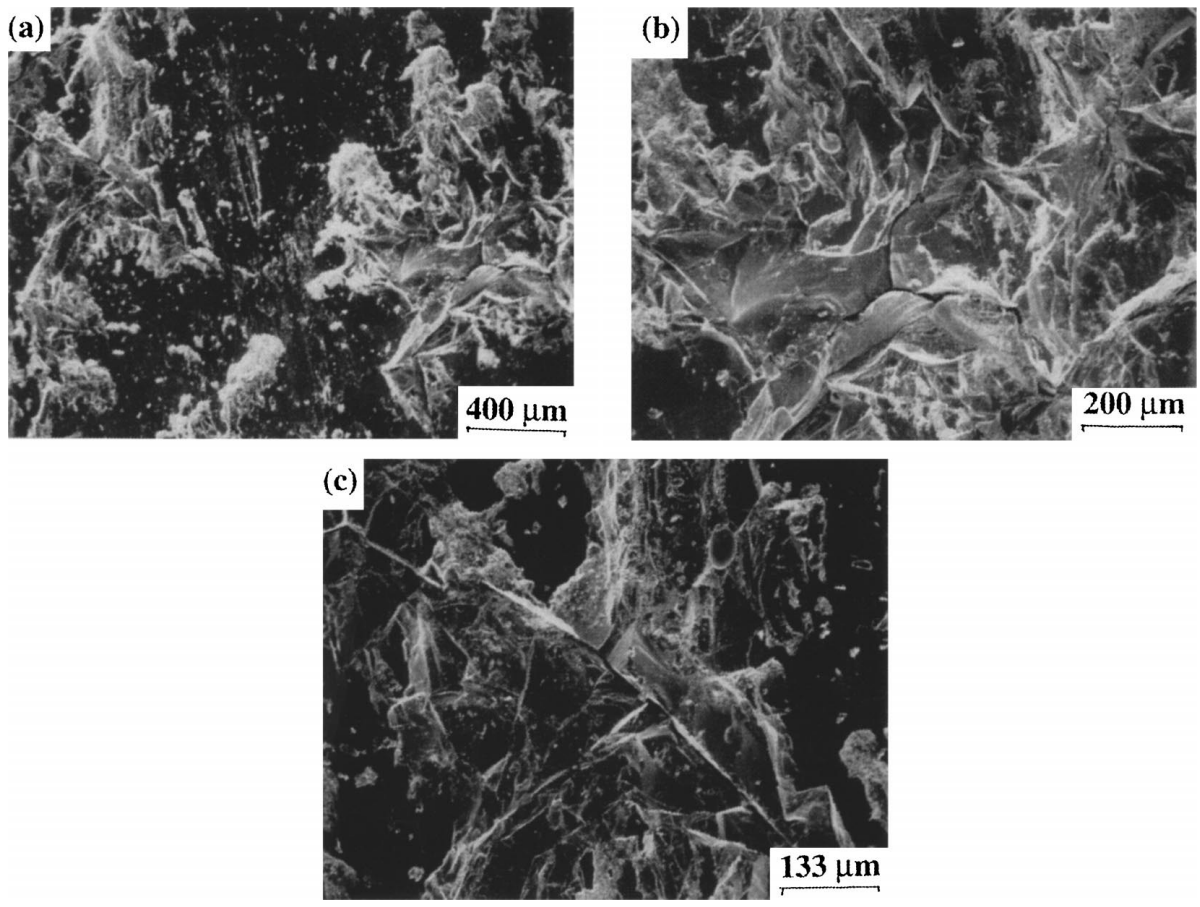

Figure 13 SEM micrographs of the sample D after it was subjected to dry sliding wear. Figures (b) and (c) are medium and high magnification views of the region in Figure (a).

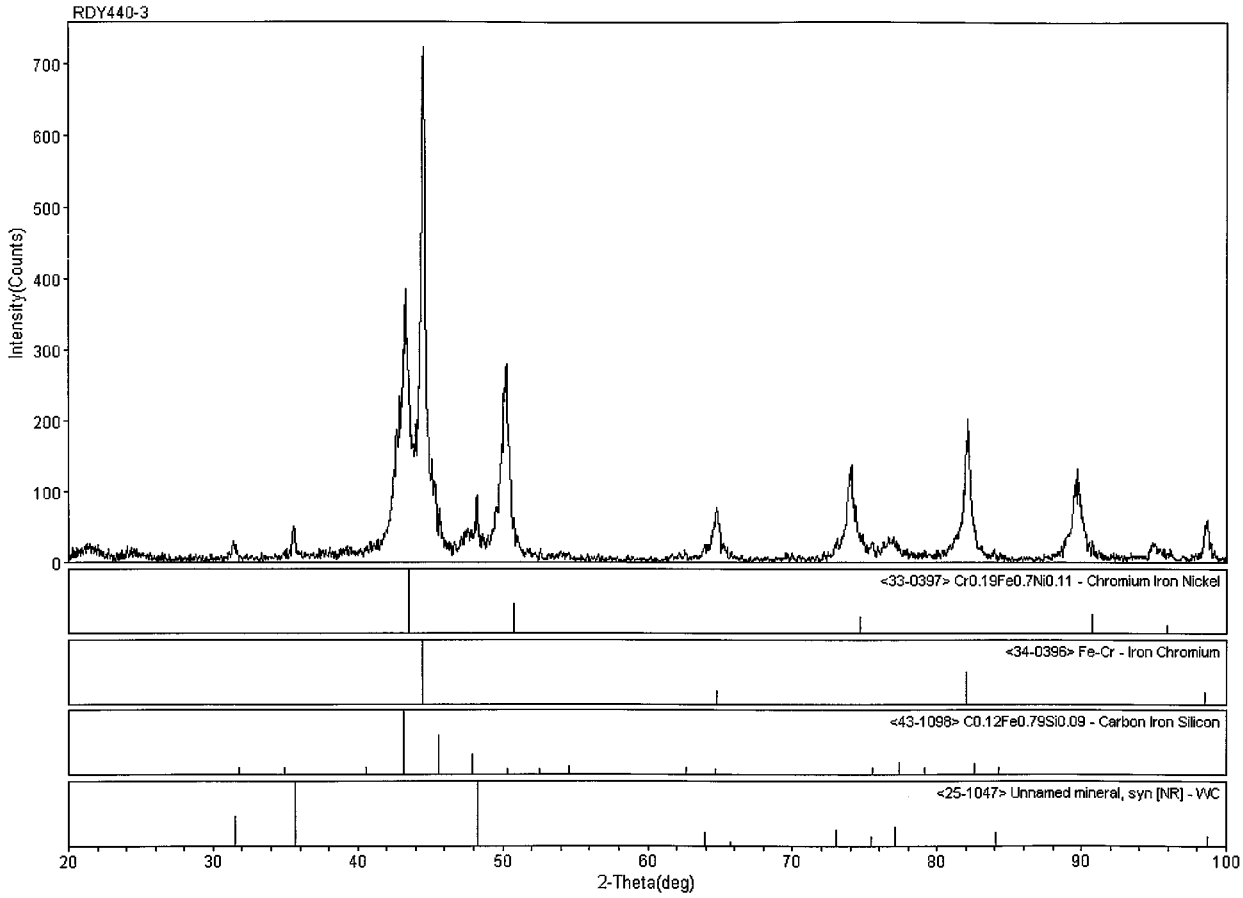

Figure 14 X-ray diffraction spectrum of worn surface of sample A.

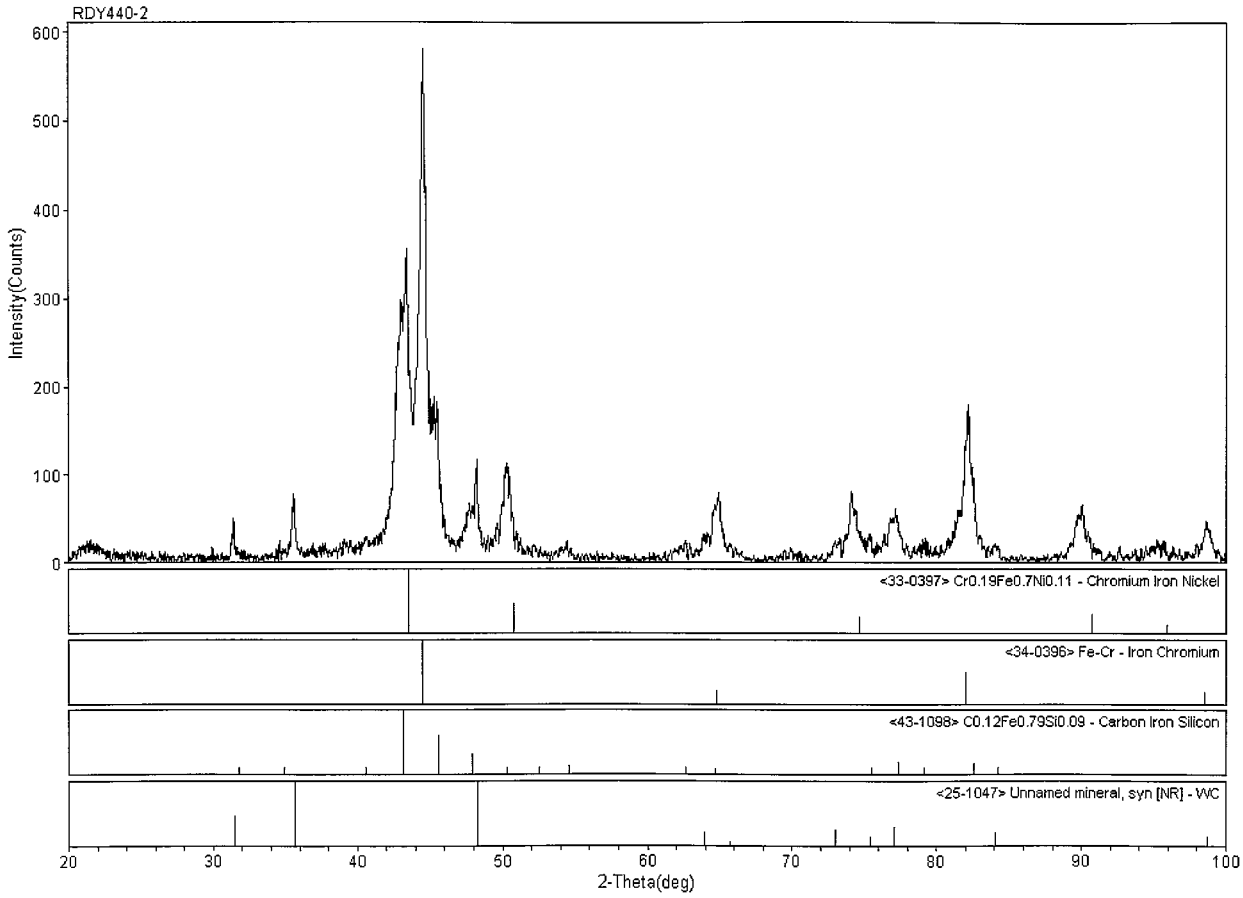

Figure 15 X-ray diffraction spectrum of worn surface of sample B.

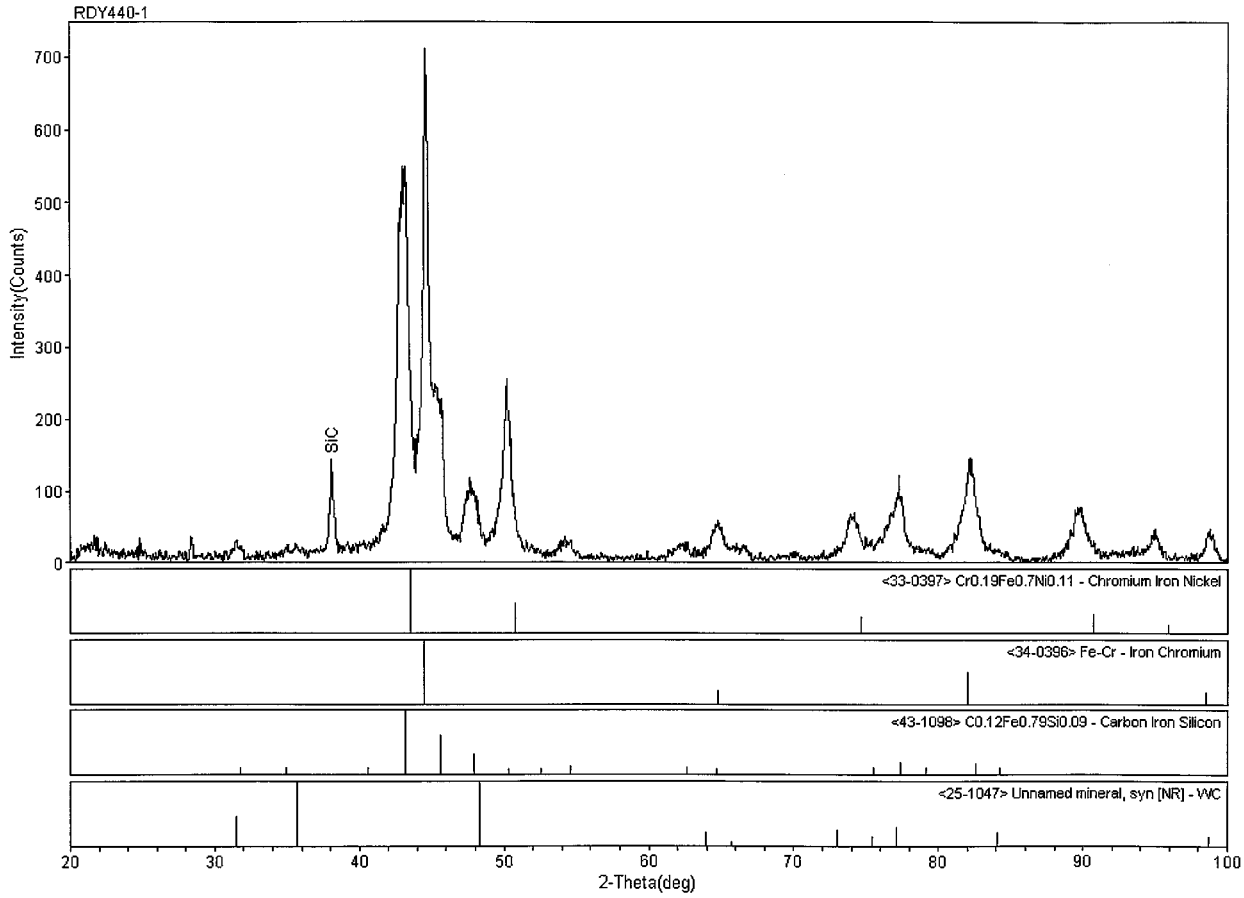

Figure 16 X-ray diffraction spectrum of worn surface of sample C.

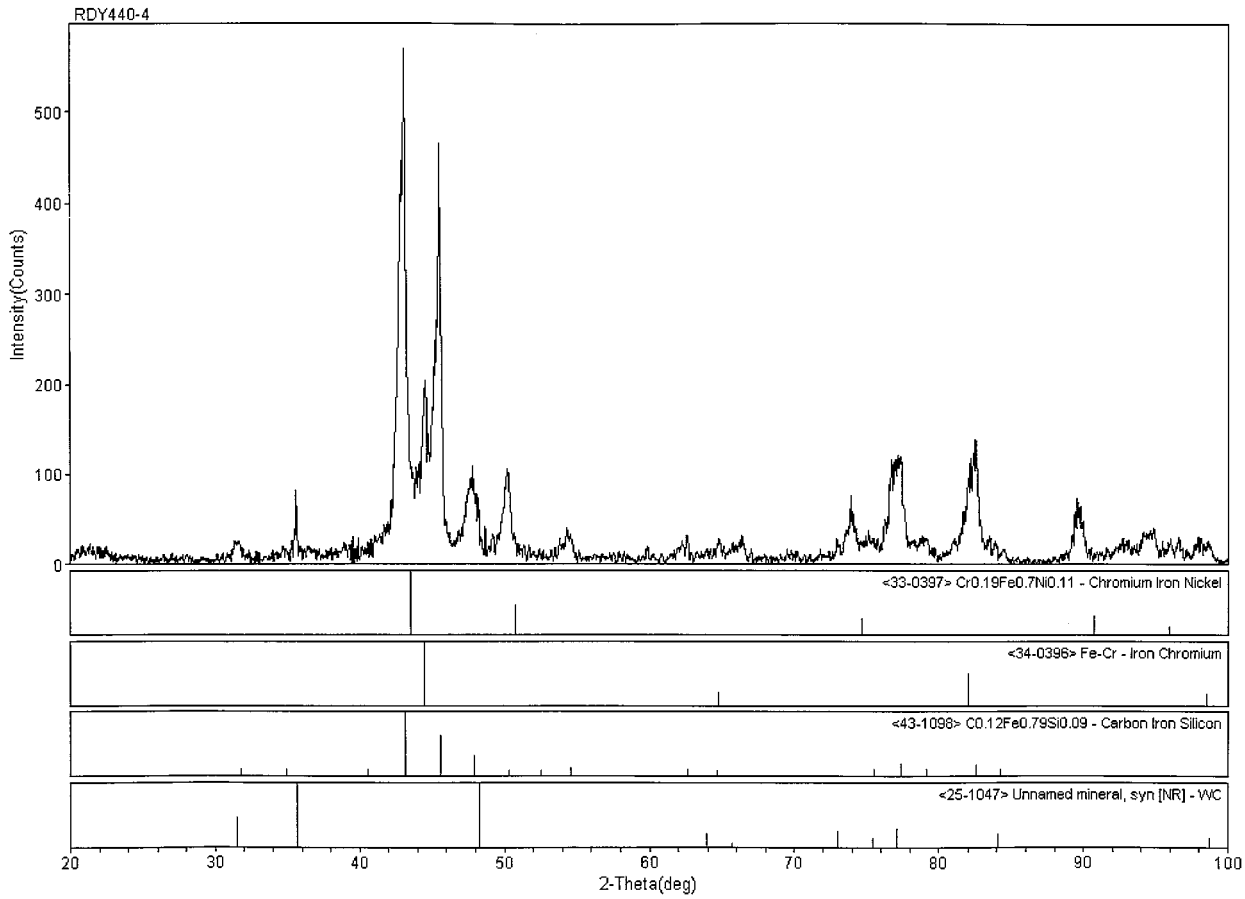

Figure 17 X-ray diffraction spectrum of worn surface of sample D.

5. Conclusions

The addition of both elements (Cr and Ni) and carbides (SiC and WC) during laser surface alloying produced competing effects in the processed layer which were not predictable using the Schaeffler diagram and properties of the respective phases and carbides. The chromium and nickel altered the matrix alloy properties, reducing the formation of hard martensite and encouraging the formation of softer austenite and ferritic phases, thus reducing the overall hardness of the processed matrix alloy, while the carbides increased the hardness. On the other hand, the corrosion resistance was improved, as was the wear resistance in two of the sets.

The carbide additions dominated the microhardness by providing an effective hardness of 2100 Knoops per weight percent addition. This negated any loss in hardness due to the elemental nickel and chromium additions and resulted in an "effective matrix hardness" of 373 Knoops. The carbides were unable, however, to prevent cracking, and it is very possible that the carbides actually initiated some of the cracks, although it is uncertain if achieving better homogeneity during processing would reduce this effect.

The reduction of some of the silicon carbide and generation of a new Fe/Si carbide produced more ferrite than anticipated due to the availability of silicon. This, in addition to the probability that the WC also partially dissociated, served to reduce the hardness of the matrix alloy and reduce the martensite content. Since the presence of some martensite is required to reduce cracking by generating compressive stresses, its absence enabled significant cracking to occur in several of the samples.

These results suggest that the improvement of both the mechanical properties, such as wear resistance and hardness, and the electrochemical properties, such as corrosion resistance, might be self-exclusive for this combination of additives due to the reduction of the carbides and the subsequent inability of the matrix to prevent cracking. At best, the chemistry of the carbide dissociation and its effect on the matrix phase structure must be considered when attempting to predict and control the processed regions.

References

1. O. V. AKGUN and O. T. INAL, *Journal of Materials Science* **30** (1995) 1605.
2. G. L. GOSWAMI, D. KUMAR, A. L. PAPPACHAN, A. K. GROVER and K. SRIDHAR, *Journal of Laser Applications* **7** (1995) 153.
3. K. STRIDHAR, A. S. KHANNA, A. GASSER and M. B. DESHMUKH, *Lasers in Engineering* **5** (1996) 107.
4. L. RENAUD, B. CHABAUD, F. FONQUET, H. MAZILLE and J. L. CROLET, *Key Engineering Materials* **46** and **47** (1990) 305.
5. N. B. DAHOTRE and K. MUKHERJE, *Journal of Materials Science* **25** (1990) 445.
6. L. G. JONNES and A. OLSEN, *Journal of Materials Science* **19** (1994) 728.
7. J. MAZUMDER and J. SINGH, "Laser Surface Alloying and Cladding for Corrosion and Wear," p. 297.
8. M. H. McCAY, N. B. DAHOTRE, J. A. HOPKINS and T. D. McCAY, *Journal of Laser Applications*, submitted .
9. A. L. SCHAEFFLER, *Metal Progress* **56** (1949) 680, 680-B .
10. J. SHEN, B. GRUNENWALD and F. DAUSINGER, in ICALEO, 1991, pp. 371–379.
11. S. M. ZHU, L. WANG, G. B. LI and S. C. TJONG, *Materials Science and Engineering* **A201** (1995) L5–L7.
12. W. D. LI and K. E. EASTERLING (1986) *Surface Engineering* **2**, 43–48.
13. M. LAMB, D. R. F. WEST and W. M. STEEN (1986) *Materials Science and Technology* **2**, 974–980.
14. G. D. RIECK, "Tungsten and its Compounds," (Pergamon Press, New York, New York, 1967) p. 80.
15. B. BHUSHAN and B. K. GUPTA, "Handbook of Tribology, Materials, Coatings and Surface Treatments," (eds.), (McGraw-Hill, Inc.) p. 453.
16. "Atlas of Isothermal Transformation and Cooling Transformation Diagrams" (American Society for Metals, Metals Park, Ohio, 1977).
17. J. SHEN, B. GRUNENWALD and F. DAUSINGER, in ICALEO, (Laser Institute of America, Orlando, FL, 1991) pp. 371–379.

Received 17 November 1998
and accepted 20 April 1999